Chapter

Experimental Determination of Thermophysical Properties of Working Fluids for ORC Applications

Christophe Coquelet, Alain Valtz and Pascal Théveneau

Abstract

The design and optimization of Organic Rankine Cycle (ORC) require knowledge concerning the thermophysical properties of the working fluids: pure components or mixtures. These properties are generally calculated by thermodynamic and transport property models (thermodynamic or equation of state or correlations). The parameters of these models are adjusted on accurate experimental data. The main experimental data of interest concern phase equilibrium properties (noncritical and critical data), volumetric properties (density and speed of sound), energetic properties (enthalpy, heat capacity), and transport properties (dynamic viscosity and thermal conductivity). In this chapter, some experimental techniques frequently used to obtain the experimental data are presented. Also, we will present some models frequently used to correlate the data and some results (comparison between experimental data and model predictions).

Keywords: working fluid design, experimental techniques, transport properties, thermodynamic properties, equations of state

1. Introduction

The utilization of energy available at low, average, and high temperature can be one solution to reduce the energy consumption particularly the fossil energy and to reduce emission of CO_2 in the atmosphere. Closed power cycle (Brayton cycle and ORC) proves to be the solution to convert heat sources into energy. Heat source can come from geothermal, solar, and biomass energy or from processes and energy systems. In general, the conditions of the heat source are fixed, and a temperature glide may be observed. In consequence, it is necessary to design the most suitable cycle architecture and to select the best working fluid in order to obtain the best performance and design of each component of the system. The selection of fluid requires thermodynamic models, and these models currently need experimental data in order to optimize their parameters. The knowledge of experimental techniques is very important to measure the thermophysical properties and to estimate their experimental uncertainties. The choice of the most suitable technique depends on the type of data to be determined, the range of pressure and temperature, the precision required, and the composition of the mixture if necessary.

In the literature several studies published concerning the investigation of working fluid for ORC applications exist. We will not present and described all the working fluid investigation. In 1985, Badr et al. [1] have examined around 68 pure working fluids (including natural fluid and hydrofluorocarbons) and given the main characteristic of the working fluids and their impacts on heat exchangers and turbine design. We can notice that in 1985, chlorofluorocarbon were not definitively banned. More recently, Saleh et al. [2] made a screening of 31 pure working fluids. They concluded that the thermal efficiency is better if the critical temperature of the working fluid is higher as possible. To increase the performance of heat exchangers and so reduce their size, Maizza and Maizza [3] suggest to use fluid with high density and high heat of vaporization. In 2012, Liu et al. [4], in the context of power generation, presented a two-stage Rankine cycle for electricity power plants. Ten pure working fluids from different chemical families (aromatics, hydrofluoroolefin, hydrofluorocarbons, hydrocarbons, ammonia) were tested. They concluded that the performance was not affected by the fluid selected. They concluded that selection would be realized on installation volume, size of the different components in the cycle, environmental protection, and operator safety. In 2017, Rahbar et al. [5] published a complete review of ORC for small-scale applications. In their paper, they present some main characteristic of the working fluid.

2. Description of Organic Rankine Cycle

An Organic Rankine Cycle is composed of a boiler/evaporator, a condenser, a pump, and a turbine (expander). The main application of ORC concerns the transformation/utilization of heat source at low or intermediate temperature (around 80°C). **Figure 1** reminds the schematic diagram of ORC. The pump compresses the liquid state working fluid until its desired pressure (and so temperature). The liquid is heated and vaporized in the boiler/evaporator which is also called the generator of vapor (the heat source). The vapor state working fluid is expanded in the turbine. During this operation electricity can be produced thanks to a generator. At low pressure, the working fluid is cooled in the condenser.

The cycle performance depends on the architecture of the system but also on the chosen working fluid and the operating conditions. The **Figure 2** presents a typical T-s diagram of an ORC with a heating and cooling medium.

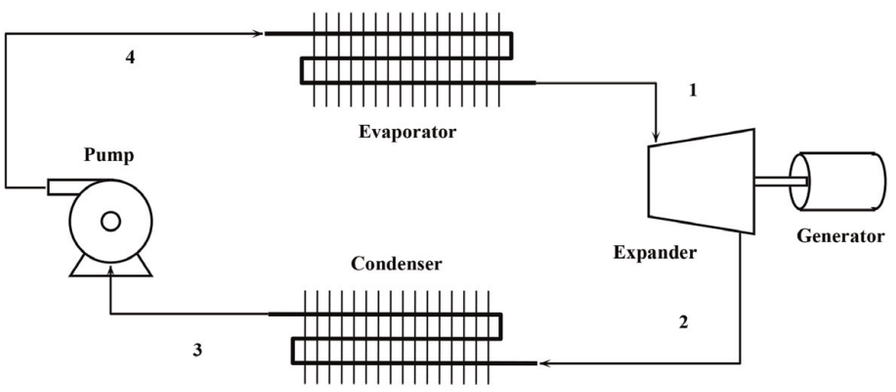

Figure 1.
Schematic diagram of ORC.

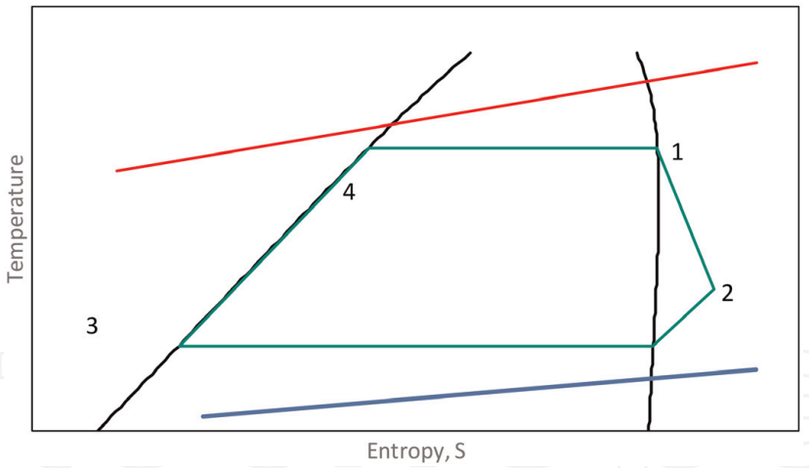

Figure 2.
Temperature-entropy diagram of the simple ORC. In green, working fluid; in red, heating medium; in blue, cooling medium.

3. Working fluid selection: characteristics

The choice of a working fluid is very crucial in the ORC systems. The working fluid should guarantee the cycle performance and system efficiency and must be adapted to the operating conditions of the system (temperature, pressure). Also hygiene, safety, and environment (HSE) aspects of the fluid have to be taken into account: the working fluid should satisfy the environment protection standards and ensure the safety of the operators. Moreover, the thermophysical properties of the working fluids impact strongly on component's size.

As the efficiency of the cycle is better for fluids with high critical temperature value [6], the working fluids are often heavy compounds with important molecular weight and low boiling point. Three types of organic fluids exist: dry, isentropic, and wet fluids. **Figure 3** presents the T-S diagrams of these fluids. For dry fluid, $dT/dS > 0$, and for isentropic fluid, $dT/dS = 0$. It signifies that during expansion, there is no formation of liquid droplet. For wet fluid, $dT/dS < 0$ (like water). During expansion, liquid droplets are formed and can damage the equipment. So, it can be necessary to add a superheating equipment.

In general, fluorinated components are used as working fluids. It is important to note that in 2014, European F-gas directive plans the prohibition of fluorinated working fluids with GWP of 2500 or more from 2020. The 2009 F-gas regulation fixes the limits of GWP for each year (Bolaji [7]). In 2018, the objective was to use fluids with GWP < 1300 close to the GWP of R134A (GWP = 1300). In 2020, the objective is to use fluids with GWP < 1000. In order to reach the objectives in terms of GWP, two solutions exist: the first one consists of the development of new fluids with low GWP values, such as hydrofluoroolefins (HFOs). The second one consists in developing new blends of refrigerants, less than four components [6]. With the existing equipment retrofit aspects are also very important. For all the cases, it is important to consider the thermophysical properties for the selection of the organic working fluid.

3.1 Chemical properties

Critical temperature: In order to guarantee ORC efficiency, the critical temperature of the chosen fluid should be as high as possible and close to the maximum temperature of the heat source.

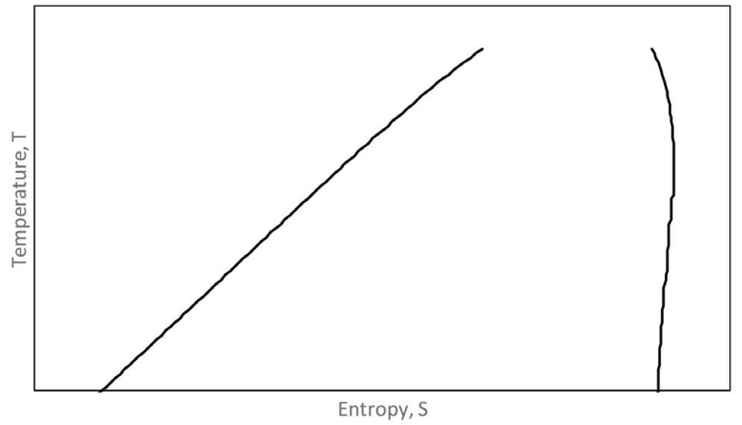

Dry

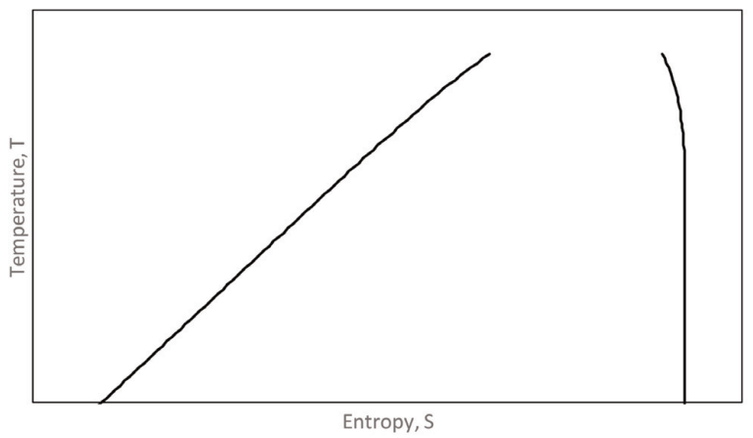

Isentropic

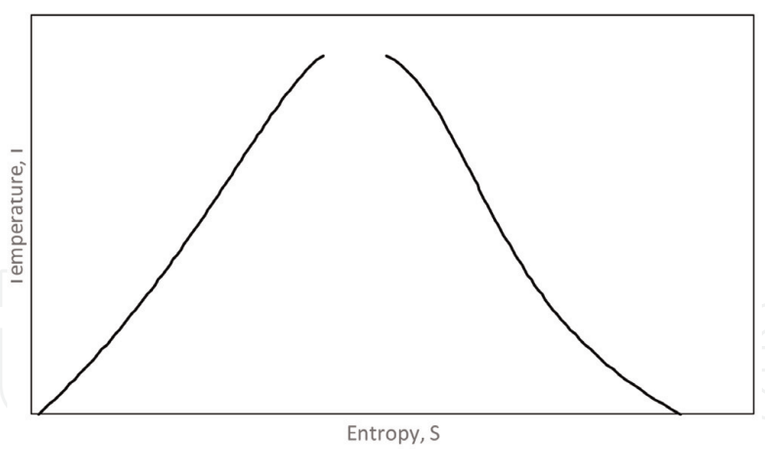

Wet

Figure 3.
Types of organic fluids (dry, isentropic, and wet) (Liu [6]).

Triple point temperature: As low as possible, the working fluid should not be freezing in ORC under low temperature condition (cold source).

Molecular weight: The larger is the molecular weight, the smaller is the specific enthalpy drop, and the lower is the number of stages required for the expander.

Thermal stability: The working fluid should not have the possibility to decompose itself under high pressure and high temperature conditions.

Safety and environment impacts: Nontoxic and non-flammable organic fluid is required to protect the personnel in case of fluid leakage. Also, the working fluid

should have zero ozone depletion potential (ODP), minimal global warming potential (GWP), and low atmospheric lifetime (ALT).

Material compatibility: The working fluid should be non-corrosive and should have a non-eroding characteristic in order to guarantee the integrity of the components of the ORC.

3.2 Thermodynamic properties

Phase diagram: The knowledge of pure component phase diagram (mainly the pure component vapor pressure) is very important in order to know the physical state of the fluid. Concerning mixtures, the phase diagrams are more complex. Recently, Privat and Jaubert [8] have revisited the Scott and van Konynenburg [9] (**Figure 4**) classification of binary systems. Depending on the temperature and pressures conditions, vapor-liquid equilibrium but also vapor-liquid-liquid equilibrium (VLLE) and liquid-liquid equilibrium (LLE) can appear.

Density and specific volume: Working fluids with low specific volume lead to low volume flow rates and so have a non-negligible impact on the sizing of heat exchangers and expanders (low volume of vapor at the outlet).

Latent heat: In general, a working fluid with high heat of vaporization is preferable as more heat is absorbed during the evaporation step. But in case of the

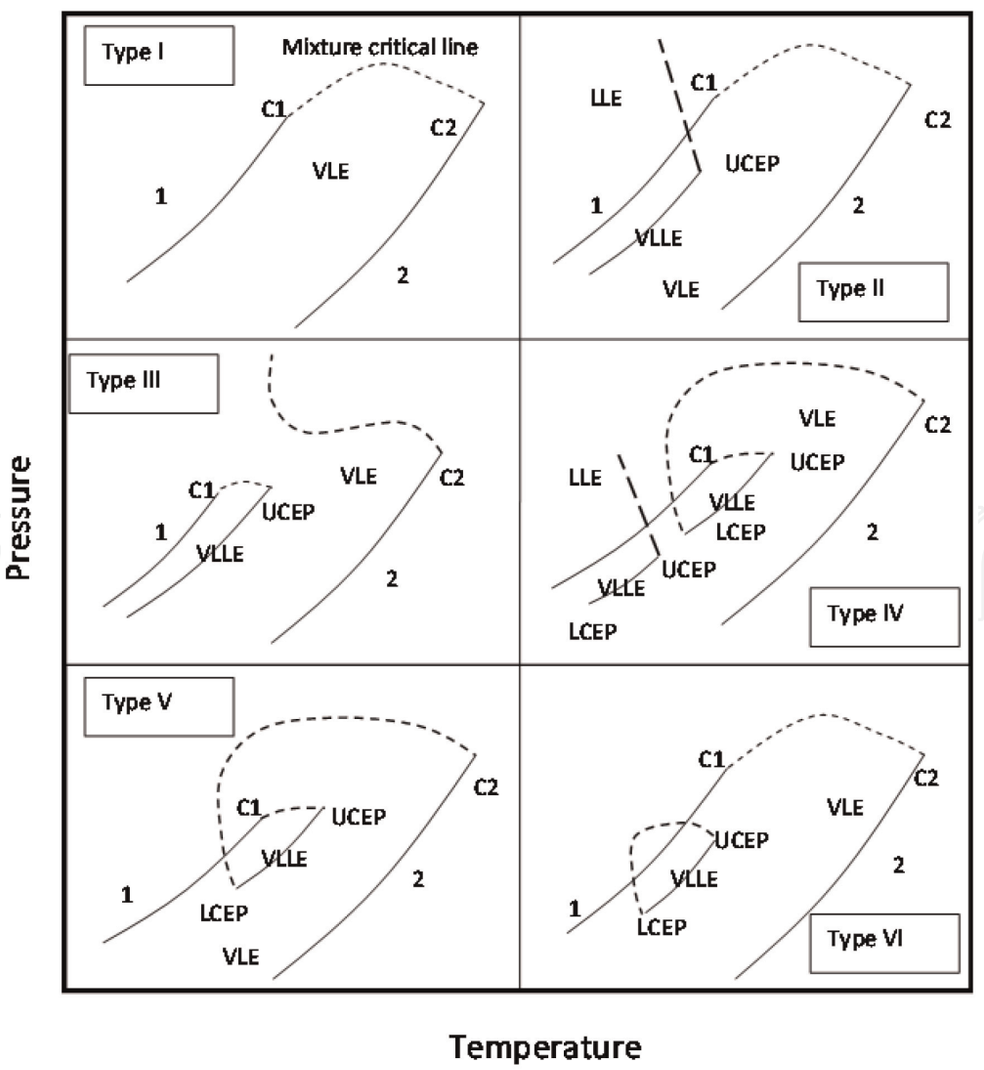

Figure 4.
Scott and van Konynenburg classification [9].

utilization of low-grade waste heat, it is better to use fluids with low latent heat of vaporization [5].

Speed of sound: The speed of the sound of the fluid limits the flow of fluid flowing in the expander. This parameter directly influences the size and therefore the cost of an ORC turbine.

The other thermodynamic properties are also useful but not crucial for the selection for the working fluid (heat capacity, surface tension).

3.3 Transport properties

Dynamic viscosity: Low dynamic viscosity for both liquid and vapor phases is preferable in order to reduce the friction losses and to maximize the heat transfer (reduction of the size of the heat exchangers, particularly heat surface exchange).

Thermal conductivity: High values of thermal conductivity are preferable in order to reduce the size of the heat exchangers (mainly surface of exchange).

4. Experimental techniques for the estimation of thermophysical properties

In this section, we will present several experimental techniques used for the experimental determination of thermodynamic and transport properties. Experimental methods for the investigation of thermophysical properties belong either to closed or open circuit methods.

Closed circuit methods: They can be divided into two main classes, depending on the method considered to determine the composition: static-analytic methods and static-synthetic methods. For the analytic methods, the composition of each phase is obtained by analyses after sampling (direct sampling method). For the synthetic methods, the global composition of the mixture is known a priori. No sampling is necessary.

Open circuit methods: There are several different techniques based on this principle. The mixture circulates through an equipment composed of sensitive element where the measurement of the thermophysical properties is realized. We can cite critical point measurement as an example of utilization of this technique. Also the densitometer technique developed by Galicia-Luna et al. [10] and Bouchot and Richon [11] which is a synthetic method can be classified as an open circuit method. A mixture with known composition circulates through a vibrating U-tube. Dynamic viscosity measurement can be also classified in this rubric.

4.1 Equilibrium properties and critical point

Synthetic or analytic methods can be considered for the determination of equilibrium properties. Vapor-liquid equilibrium properties can be obtained using the "static-analytic" method. Herein, the mixture is enclosed in an equilibrium cell equipped with a mixing mechanism to get fast equilibrium conditions. When the equilibrium is reached, small quantities of the phases are sampled and analyzed through chromatographic analyzers. A complete description of the setup is available in Wang et al.'s [12] paper. The apparatus is similar to the one present on **Figure 5**. Capillary samplers like ROLSI™ (Armines's patent) can be used to take samples.

The variable volume cell technique (**Figure 6**) can be cited as a static-synthetic method [13, 14]. The components of the mixture are introduced separately, and the composition is known by weighing procedure or after analysis. The volume of the cell is modified with a piston to study bubble points. At fixed temperature, saturating

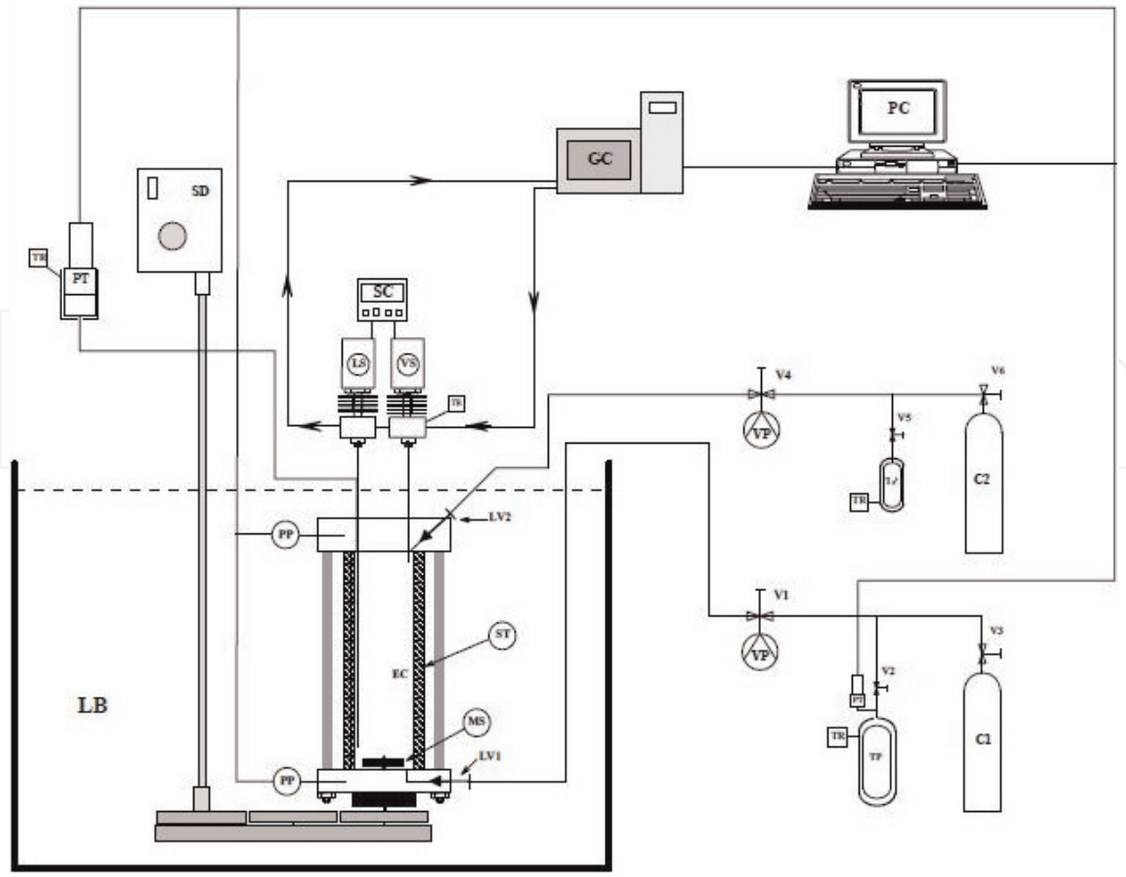

Figure 5.
Schematic diagram of the static-analytic apparatus. EC, equilibrium cell; LV, loading valve; MS, magnetic stirrer; PP, platinum resistance thermometer probe; PT, pressure transducer; RT, temperature regulator; LB, liquid bath; TP, thermal press; C1, more volatile compound; C2, less volatile compound; V, valve; GC, gas chromatograph; LS, liquid sampler; VS, vapor sampler; SC, sample controlling; PC, personal computer; VP, vacuum pump.

properties (pressure and saturated molar volume) of the mixture are determined through the pressure vs. volume curve recorded that displays a break point.

Isochoric method (**Figure 7**) can be used also to measure the dew point of multicomponent system. The components of the mixture are introduced separately, and the composition is known by weighing procedure or after analysis. The mixture is introduced at its vapor state, and then the temperature slowly decreases. The pressure and temperature are recorded. When the first drop of liquid appears, a break in the P-T curve is observed. The break point corresponds to the dew point. This technique is identical to the technique used to determine gas hydrate dissociation points [15].

Concerning critical point measurement, it is necessary to use a special device. The technique is based on dynamic-synthetic method where the mixture is circulating through the equilibrium cell (**Figure 8**) under specific conditions of temperature and pressure. A critical point can be determined by visually observing the critical opalescence and the simultaneous disappearance and reappearance of the meniscus, i.e., of the liquid-vapor interface from the middle of the view cell.

4.2 Volumetric properties or densities

It is well known that density is required for the development of equations of state and the development of models for mass and heat transfers. Several techniques which can be used to measure the density exist. We can cite the hydrostatic balance densitometer coupling with magnetic suspension (single-sinker method from Wagner et al. [16]), density measurement with vibrating bodies, bellows [17], and

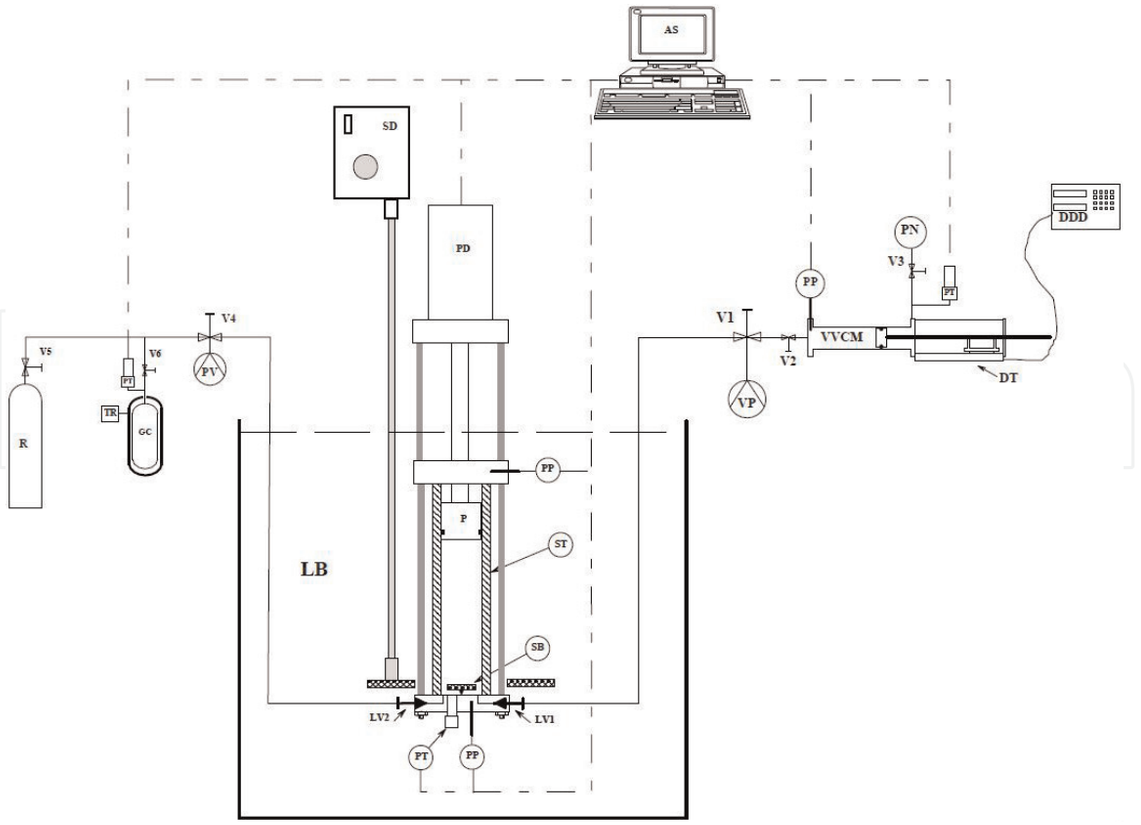

Figure 6.
Example of equipment which can be used for bubble point measurement. DAU, data acquisition unit; DDD, digital displacement display; DT, displacement transducer; GC, gas cylinder; LB, liquid bath; LVi, loading valve; P, piston; PM, piston monitoring; PN, pressurized nitrogen; PP, platinum probe; PT, pressure transducer; PV (VP), vacuum pump; R, gas reservoir; SD, stirring device; SB, stirring bar; ST, sapphire tube; TR, thermal regulator; Vi, valve; VVCM, variable volume cell.

isochoric method [18]. More details concerning these techniques of measurements (and others) are detailed in the IUPAC book dedicated to experimental thermodynamics [19]. Herein, we will only describe the technique based on vibrating tube densitometer.

A mixture with known composition can circulate through a vibrating U-tube (static or dynamic mode). Density is deduced from careful calibration using reference fluids. This apparatus can be used to obtain (PρT) data of compressed phases. A complete description of this technique is available in the papers of Coquelet et al. [20]. This technique is not very recommended close to the critical point. In effect, vibration of the tube may provoke a phase transition. Other techniques based on isochoric method can be used also to determine the volumetric properties at the vicinity of the critical point [21] (**Figure 9**).

4.3 Speed of sound

The speed of sound data is also very important to determine the equation of state, and it is linked to other thermodynamic properties. In effect, the isothermal compressibility κ_T is related to the isentropic compressibility κ_S via Maxwell's relations (Eq. (1)):

$$\kappa_T = \kappa_S + \alpha^2 v \frac{T}{C_p} \tag{1}$$

In Eq. (2), v [m^3/mol] is the molar volume of the compound, Cp is the heat capacity [J/mol], and κ_S is the isentropic compressibility $\kappa_S = -\frac{1}{v}\left(\frac{\partial v}{\partial P}\right)_S$ [Pa^{-1}] and is determined thanks to the measurements of speed of sound c [m/s] and density

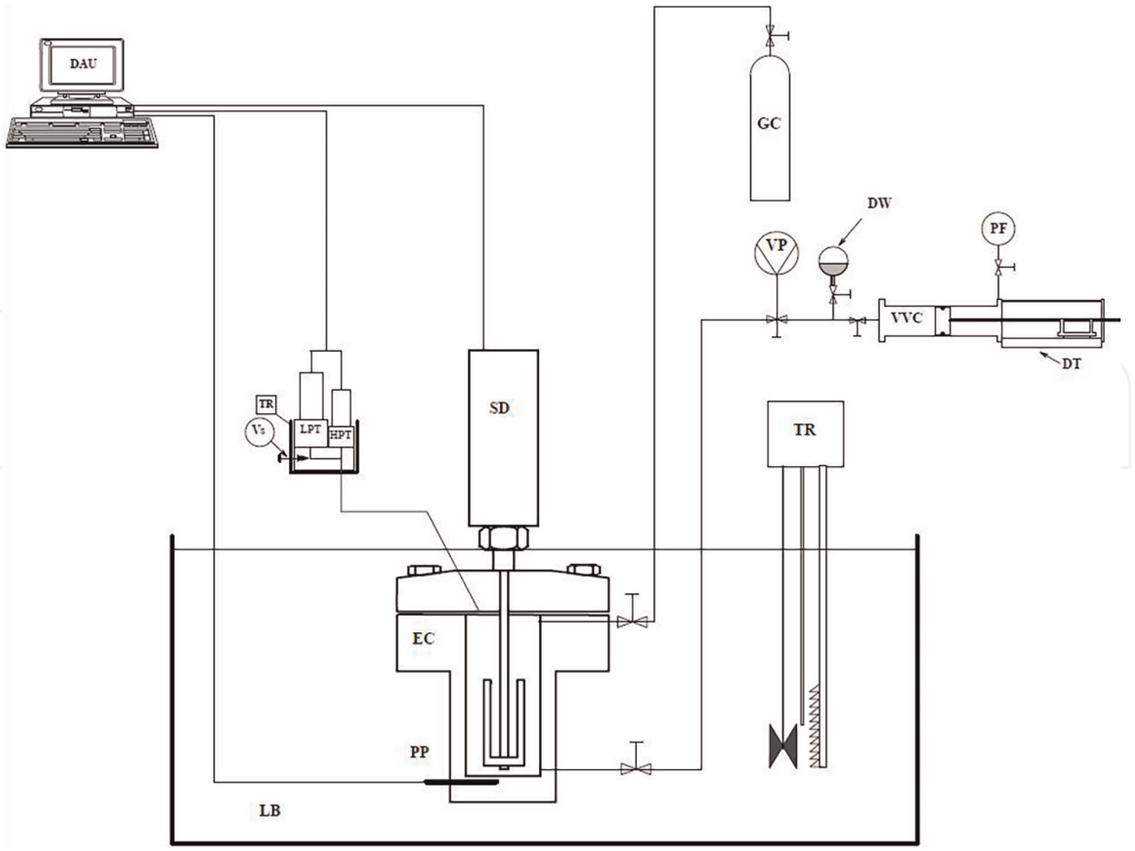

Figure 7.
Example of equipment which can be used for dew point measurement. DW, degassed water; DAU, data acquisition unit; EC, equilibrium cell; GC, gas cylinder; LPT, low pressure transducer; LPT, high pressure transducer; LB, liquid bath; PP, platinum probe; SD, stirring device; TR, temperature regulator; VP, vacuum pump; VVC, variable volume cell; PF, pressurizing fluid; DT, displacement transducer.

ρ [kg/m^3] reached in this work. Indeed, these three properties are linked in the liquid phase via $c = \sqrt{\frac{1}{\kappa_S \rho}}$. Like with density measurement, several techniques which were developed to obtain the value of speed of sound exist. The spherical resonator developed by Mehl and Moldover [22] (with high accuracy in gases), Trusler and Zarari [23], and Benedetto et al. [24] can be cited as example. For liquid and dense fluid, pulse-echo techniques are preferred for measuring the speed of sound particularly at high pressure. More details concerning these techniques of measurements (and others) are detailed in the IUPAC book dedicated to experimental thermodynamics [19]. Herein, we will describe one technique used at Heriot-Watt University [25]. **Figure 10** describes the cell of measurement. A cylindrical acoustic cell with well-known dimension is considered to measure the sound speed in the fluid using through-transmission method of ultrasonic testing. In this method, a transducer is located on one side of the cell, and a detector is placed on the opposite side of the acoustic cell (electric signal is converted into ultrasound waves and vice versa). An oscilloscope is used to observe the waves. Speed of sound is obtained by dividing the period of the waves by the distance between the speed of sound transducer and detector.

4.4 Heat capacity

The determination of isobaric heat capacity is done using a differential scanning calorimeter (DSC). The equipment is composed of two cells: one is the measurement cell, and one is the reference cell. A sample is introduced into the measurement cell, and a temperature ramp is applied. Knowing the heat flux transferred (absorbed or released, $\phi = \left(\frac{\partial H}{\partial t}\right)$) and the ramp, it is possible to estimate the heat capacity (Eq. (2)):

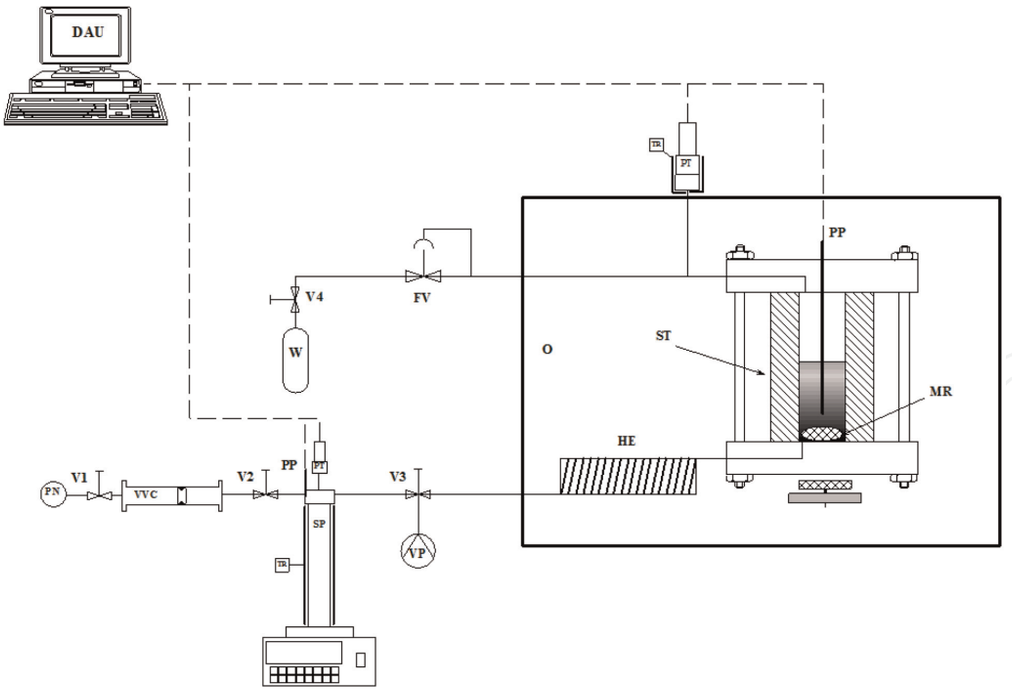

Figure 8.
Schematic diagram of the critical point measurement apparatus. DAU, data acquisition unit; FV, flow regulation valve; HE, heat exchanger; MR, magnetic rode, O, oven; PN, pressurized nitrogen; PP, platinum probe; PT, pressure transducer; ST, sapphire tube; SP, syringe pump; TR, temperature regulator; Vi, valve; VVC, variable volume cell; VP, vacuum pump; W, waste.

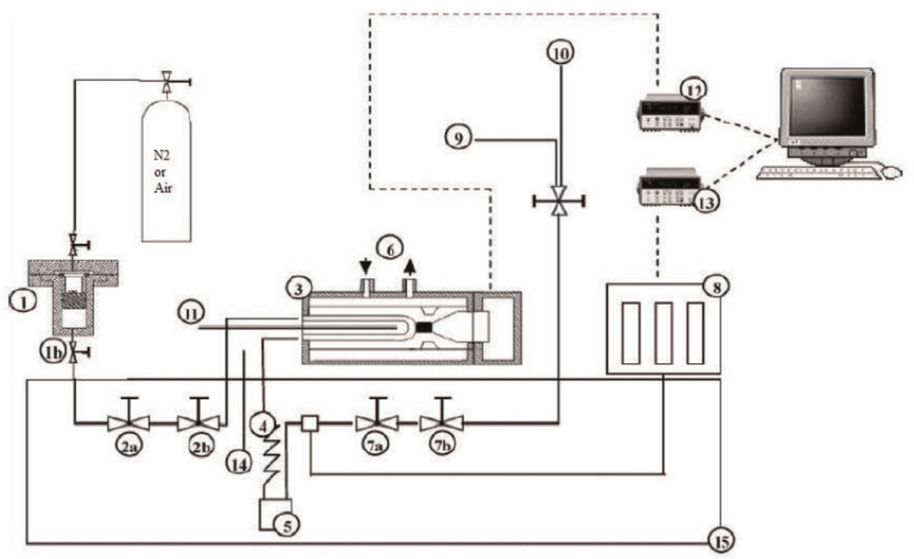

Figure 9.
Flow diagram of the vibrating tube densimeter [20]. (1) loading cell, (2a and 2b) regulating and shutoff valves, (3) DMA-512P densimeter, (4) heat exchanger, (5) bursting disk, (6) inlet of the temperature regulating fluid, (7a and 7b) regulating and shutoff valves, (8) pressure transducers, (9) vacuum pump, (10) vent, (11) vibrating cell temperature probe, (12) HP 53131A data acquisition unit, (13) HP34970A data acquisition unit, (14) bath temperature probe, (15) principal liquid bath.

$$C_P = \phi \Big/ \left(\frac{\partial T}{\partial t}\right) \tag{2}$$

In Eq. (4), H is the enthalpy, T is the temperature, and t is the time. A complete description of this technique is available in the paper of Al Ghafri et al. [26]. **Figure 11** presents a short description of the technique.

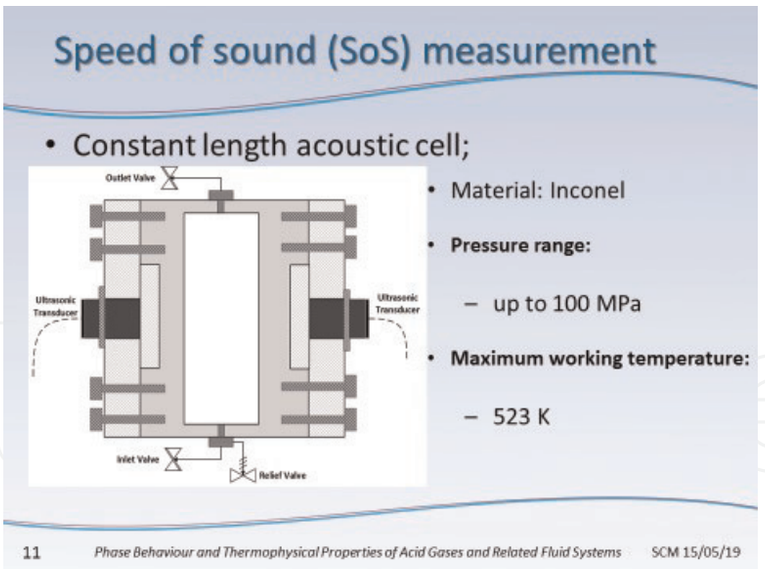

Figure 10.
View of the acoustic cell of equipment designed by Ahmadi et al. [25].

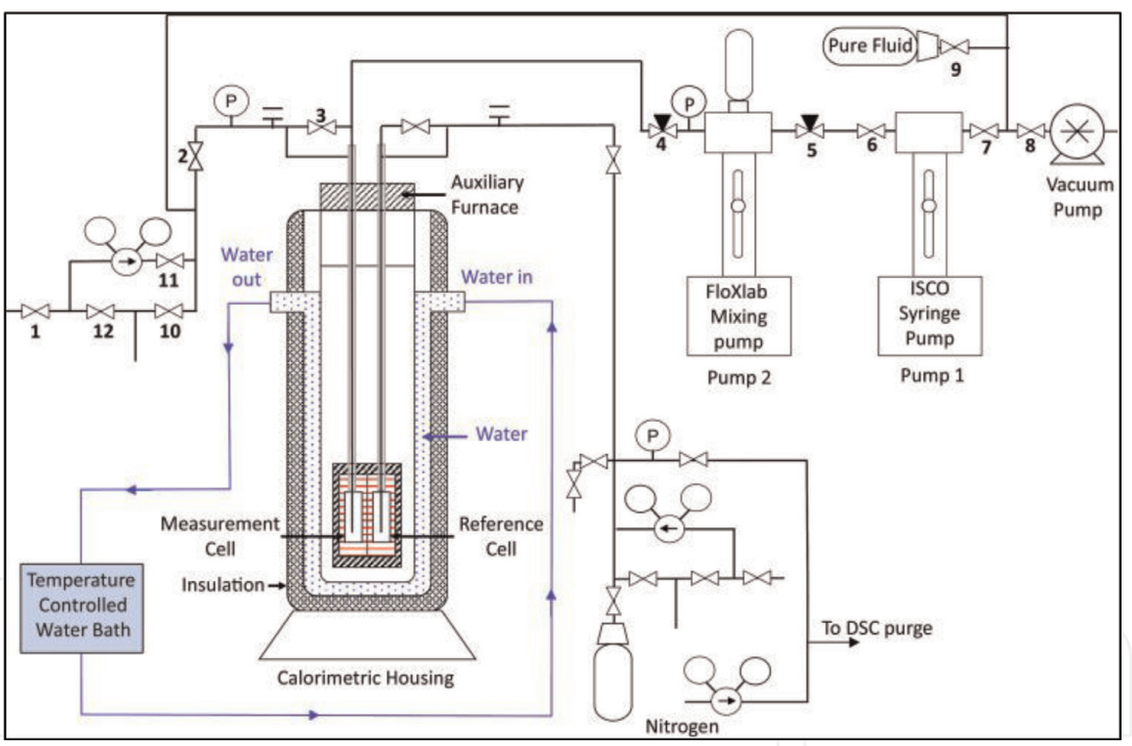

Figure 11.
Differential scanning calorimeter used for measurements of the isobaric heat capacities of liquid refrigerant mixtures from Al Ghafri et al. [26].

4.5 Transport properties

4.5.1 Interest of transport properties in engineering

Chemical and mechanical engineers use correlations with nondimensional numbers (Eq. (3)) to estimate heat transfer coefficient (h) essential for the estimation of global heat transfer coefficient of the heat exchanger and so the design of heat exchangers:

$$Nu = A\mathrm{Re}^{\alpha}\mathrm{Pr}^{\beta} \tag{3}$$

In Eq. (1), Nu is the Nusselt number $Nu = \frac{hL}{\lambda}$, Re is the Reynolds number $\mathrm{Re} = \frac{\rho v L}{\mu}$, and Pr is the Prandtl number $\mathrm{Pr} = \frac{C_p \mu}{\lambda}$ with h being the heat transfer coefficient [$J.m^{-2}$], L a characteristic length [m], λ the thermal conductivity [$J.m^{-1}$], ρ the density [$kg.m^3$], μ the viscosity [Pa.s], Cp the heat capacity [$J.mol^{-1}.K^{-1}$], and v the speed of the fluid [$m.s^{-1}$]. The correlation can be modified with the utilization of Weber number ($We = \frac{\rho L v^2}{\gamma}$, γ is the surface tension) taking into account the effect of interfacial tension during the formation of the bubble of gas in the evaporator or drop of liquids in the condenser.

We remind that for a heat exchanger, global heat transfer coefficient (U) depends on the local heat transfers (h) of the two fluids and the thermal conductivity of the material of the heat exchanger.

4.5.2 Dynamic viscosity

Like density measurements, several techniques to determine viscosity of fluids exist. For example, we can cite the falling ball technique [27], capillary technique, vibration quartz [28], and vibrating bodies [29, 30]. We invite the reader to have a look in the paper from Le Neindre [31] for a complete overview of the techniques of measurement. Herein we will only describe the viscometer used to measure dynamic viscosities using the capillary tube viscosity method. A schematic view of the setup used at Heriot-Watt University is shown in **Figure 12**. The apparatus is

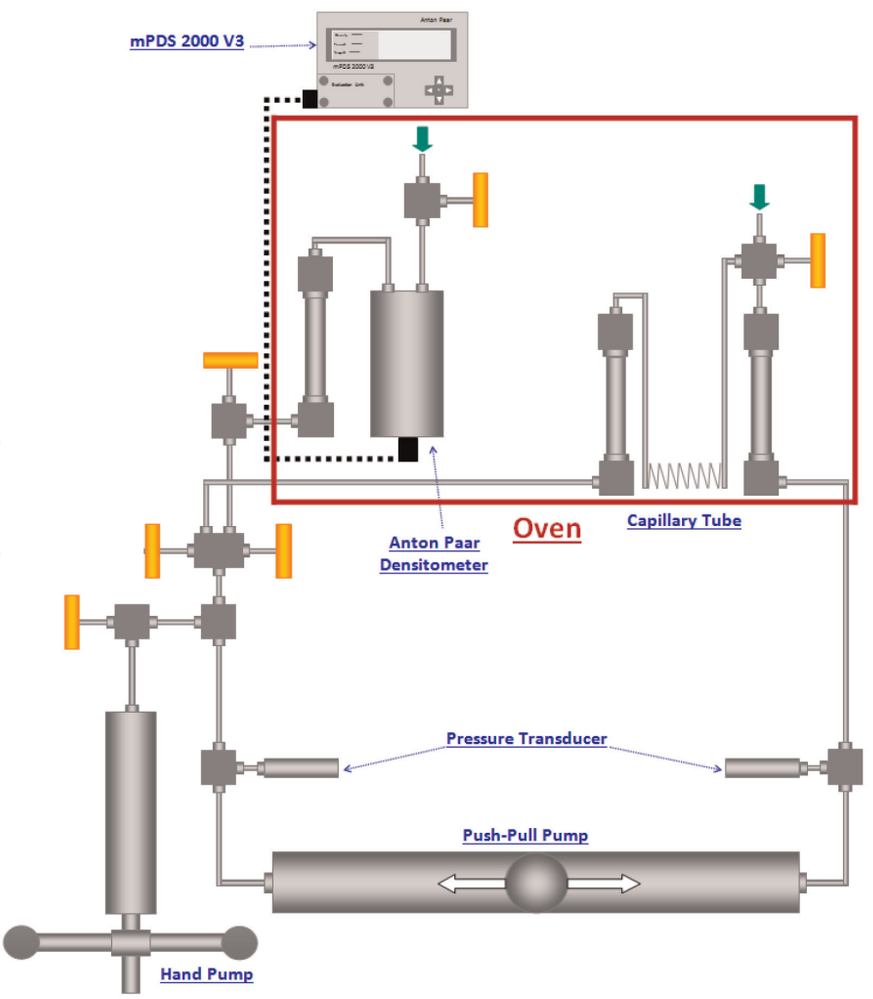

Figure 12.
Schematic diagram of the setup used for dynamic viscosity measurement [32].

comprised of two small cylinders connected to each other through a capillary tube and a temperature-dependent calibrated internal diameter. A complete description of this technique is available in the paper of Kashefi et al. [32]. The temperature of the system was set to the desired condition, and the desired pressure was set using the hand pump. Poiseuille equation (Eq. (4)) (in laminar flow conditions) can relate the pressure drop across the capillary tube to the viscosity, tube characteristics, and also flow rate for laminar flow:

$$\Delta P = \frac{128LQ\mu}{C\pi D^4} \tag{4}$$

In Eq. (3), ΔP is the differential pressure across the capillary tube viscometer in psi, Q represents the flow rate in cm^3/sec, L is the length of the capillary tube in cm, D refers to the internal diameter of the capillary tube in cm, μ is the dynamic viscosity of the flown fluid in cP, and C is the unit conversion factor equal to 6,894,757 if the above units are used.

4.5.3 Thermal conductivity

Several techniques exist to measure the thermal conductivity of fluids [33]. Among those methods, the transient hot-wire method is considered to be the most used technique and to be a very accurate and reliable technique to measure this thermophysical property. The basic theory of the transient hot-wire method is presented in Healy's paper [34], and procedure of measurement is fully described in the paper of Marsh et al. [35]. Generally, a transient hot-wire apparatus consists of one highly pure platinum wire, a current source, a voltage meter, a data acquisition system, and a computer (**Figure 13**). The current source provides a constant current for the platinum wire, which is embedded in the tested fluid. Then the temperature of the wire will rise because of the Joule effect. Subsequently, the temperature of the

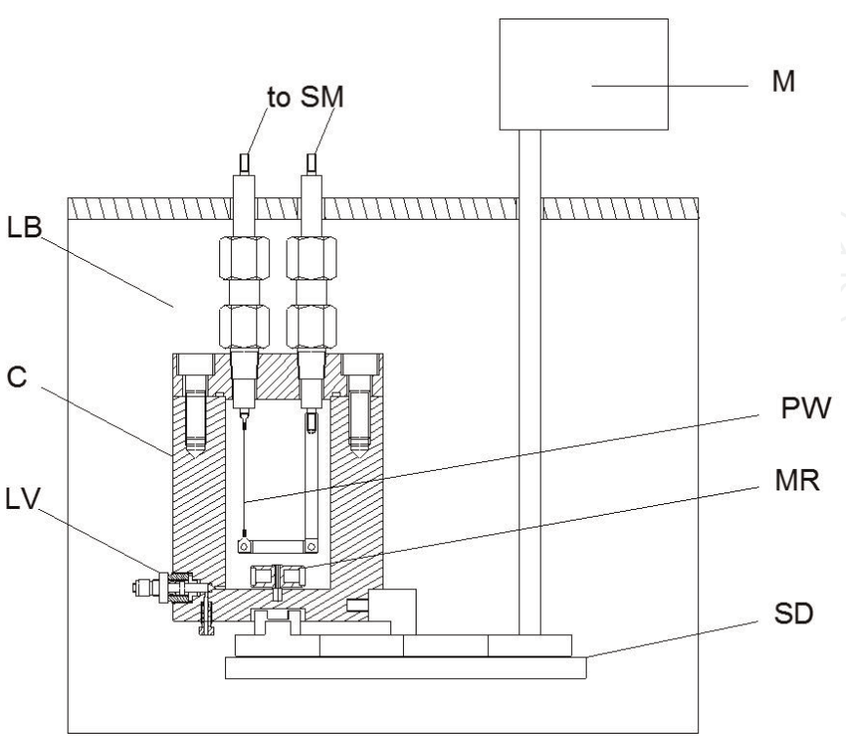

Figure 13.
View of the thermal conductivity cell (hot-wire method). LB, liquid bath; C, cell; LV, loading valve; M, motor; PW, platinum wire; MR, magnetic rod; SD, stirring device; to SM, to SourceMeter.

fluid will also change as a result of the heat conduction between the wire and the fluid (heat radiation and convection are in general neglected). The temperature rise of the platinum wire as a function of the duration t is given by Eq. (5):

$$\Delta T = \frac{q}{4\pi\lambda} \ln\left(\frac{4\kappa t}{r^2 C}\right) \tag{5}$$

In Eq. (5), λ is the thermal conductivity of the sample, q is the constant power provided to the wire, W/m. κ is the thermal diffusivity of the fluid, r is the radius of the hot wire, and C is Euler's constant, whose value is 1.781. As the relation between the ΔT and ln(t) can be determined through the experiments, the thermal conductivity of the tested fluid can be calculated using this equation. Compared with other methods, the convenience, accuracy, and the short duration of transient hot-wire method make it a widely used method nowadays.

5. Data treatment

Process or system simulator required models or correlation in order to define the best operating conditions (T, P, flow, compositions) with the maximum of efficiency and the best coefficient of performance (COP) but also to design each component (heat exchangers, expanders, valves, expander). In this section we will just present few models which can be used with the experimental data in order to predict the phase diagrams and thermodynamic and transport properties.

5.1 Thermodynamic models

In this section, we propose a presentation of three types of thermodynamic models. These models are briefly described. The main difference concerns the number of parameters we have to adjust and so the quantity and type of experimental data we have to acquire in order to adjust the parameters.

The thermodynamic properties are obtained by using equations of state (EoSs). In the process simulators, the most famous EoSs are of cubic type, such as Eq. (6):

$$P = \frac{RT}{v-b} - \frac{a\alpha(T)}{v^2 + uvb + wb^2} \tag{6}$$

In Eq. (6), R is the ideal gas constant, a and b are the parameters of the EoS calculated using the critical temperature (Tc) and pressure (Pc) of each component, and α(T) is a function of temperature, acentric factor, Tc, and Pc. u and w are other parameters.

Another type of equation of state of the molecular type can be used. The Helmholtz energy is calculated by considering all the molecular interactions like dispersion, polarity, H bonding (association), etc. Equation (7) describes the method of calculation of the Helmholtz energy A:

$$\frac{A}{Nk_bT} = \frac{A^{\text{Ideal}}}{Nk_bT} + \frac{A^{\text{Segment}}}{Nk_bT} + \frac{A^{\text{Chain}}}{Nk_bT} + \frac{A^{\text{Association}}}{Nk_bT} \tag{7}$$

In Eq. (7), k_b is the Boltzmann constant, T is the temperature, and N is the mole number. The most known molecular EoSs of this type are SAFT type. Based on the Wertheim's statistical theory of associative fluids (1984), Chapman et al. [36]

developed the first EoS SAFT (statistical associating fluid theory) called SAFT-0. Many versions exist today, such as SAFT-VR [37], PC-SAFT [38], and SAFT Mie [39]. The various versions differ mainly in the choice of the reference fluid, the radial distribution function, and explicit expressions of the terms of perturbation.

The last type of equation of state which can be used to estimate the thermodynamic properties is based on multi-fluid approximation. It is well known that from the knowledge of Helmholtz energy, all thermodynamic properties can be calculated. This equation of state is explained in terms of reduced molar Helmholtz free energy (Eq. (8)). Temperature and density are expressed in the dimensionless variables $\delta = \frac{\rho}{\rho_C}$ and $\tau = \frac{T}{T_C}$:

$$\frac{A(T_r, \rho_r, \overline{x})}{RT} = a(T_r, \rho_r, \overline{x}) = a^{id}(T_r, \rho_r, \overline{x}) + a^{res}(T_r, \rho_r, \overline{x}) \tag{8}$$

In Eq. (8), the exponent "id" stands for the ideal gas contribution, and exponent "res" is the residual contribution. ρ_r and T_r are the reduced density and temperature, respectively. Concerning the development of equation of state for the mixtures, the first possibility is to consider mixing rules for each parameter like in the cubic equation of state. The best approach is to consider the multi-fluid approximation. This approach was introduced by Tillner-Roth in 1993 [40]. It applies mixing rules to the Helmholtz free energy of the mixture of components (Eq. (9)):

$$\begin{aligned} a(T_r, \rho_r, \overline{x}) = \frac{A(T_r, \rho_r, \overline{x})}{RT} &= \sum_j x_j \left(a_j^{id}(T_r, \rho_r) + a_j^{res}(T_r, \rho_r) \right) + x_j \ln x_j \\ &+ \sum_{p=1} \sum_{q=p+1} x_p x_q F_{pq} a_{pq}^E \end{aligned} \tag{9}$$

In Eq. (9), superscript "E" is for excess properties, and subscripts "p," "q," and "j" are the component index. An excess property is defined to calculate the deviation from ideal mixture. $\Delta a_{pq}^{res} = \sum_{p=1} \sum_{q=p+1} x_p x_q F_{pq} a_{pq}^E$ is called departure function from the ideal solution. It is an empirical function, like Eq. (10), fitted to experimental binary mixture data, mainly densities, speed of sound, or heat of mixing. In this departure function, the F_{pq} parameters take into account the behavior of one binary pair with another. If only vapor-liquid equilibrium properties are available, a_{pq}^E can be considered to be equal to zero [41]:

$$\frac{A(T_r, \rho_r)}{RT} = \ln(\delta) + \sum_i \alpha_i \tau^{t_i} + \sum_k \alpha_k \tau^{t_k} \delta^{d_k} \exp\left(-\gamma \delta^{l_k}\right) \tag{10}$$

Equation (10) contains several adjustable parameters α_i, α_k, t_k, d_k, and l_k. Experimental data is required to adjust these parameters. Moreover, if $l_k = 0$, then $\gamma = 0$ and if $l_k \neq 0$, then $\gamma = 1$.

With the multi-fluid approximation, it is important to calculate the new critical properties corresponding to the mixture studied (superscript "mix") because reduced parameters are used in Eq. (8).

For example, we can use $T_C^{mix} = \sum_{p=1} \sum_{p=1} k_{T,pq} x_p x_q \left(T_{Cp} T_{Cq}\right)^{0.5}$ and $v_C^{mix} = \sum_{p=1} \sum_{p=1} k_{v,pq} x_p x_q \frac{1}{8} \left(\left(v_{Cp}\right)^{1/3} + \left(v_{Cq}\right)^{1/3} \right)^3$ where $k_{T,pq}$ and $k_{v,pq}$ are adjustable binary interaction parameters. VLE data should be used to fit $k_{T,pq}$ parameters, and if experimental data concerning densities of mixture are available, it is possible to fit $k_{v,pq}$.

5.2 Transport property models

Concerning the transport properties, different approaches exist. One consists in using the corresponding state method. The most famous approach is the TRAPP method developed by the NIST. Huber et al. [42] and Klein et al. [43] have developed a series of equations adapted to the prediction of viscosities and thermal conductivities of pure components and mixtures. The approach consists in modifying the transport properties in the ideal dilute gas state taking into account the molecular interactions (and so the density of the fluid with temperature and pressure).

The viscosity of a dilute gas can be determined as a function of temperature by Eq. (11). A dilute gas is composed by noninteractive rigid spheres of diameter σ:

$$\eta^{\circ} = C\frac{T^{\frac{1}{2}}M^{\frac{1}{2}}}{\sigma^2} \tag{11}$$

In Eq. (11), T is temperature in K, M is the molar mass in g/mol, σ is the diameter of the rigid sphere in nm, and C is a constant depending of the molecule considered. Chapman-Enskog cited in Poling and Prausnitz [44] have introduced an additional term called "collision integral" which takes into account the collision between the molecules (Eq. (12)):

$$\eta^{\circ} = K\frac{T^{\frac{1}{2}}M^{\frac{1}{2}}}{\sigma^2\Omega} \tag{12}$$

In Eq. (12), $\ln(\Omega) = \sum_i a_i \left(\ln\left(\frac{T}{\frac{\varepsilon}{k}}\right)\right)^i$, and ?/k is an empirical factor link to the potential of interaction.

Concerning thermal conductivity, λ_0(T) represents the dilute gas thermal conductivity and can be calculated by Eq. (13):

$$\lambda_0 = A_1 + A_2(T/T_C) + A_3(T/T_C)^2 \tag{13}$$

When the pressure and so the density of the fluid increases, molecular interaction between molecules cannot be neglected, and so it is necessary to apply a correction (like a residual term for equation of state). Equations (14) and (15) lead to calculate dynamic viscosity and thermal conductivity:

$$\eta = \eta^{\circ} + \Delta\eta \tag{14}$$

In Eq. (14), $\Delta\eta$ is the residual viscosity:

$$\lambda(\rho, T) = \lambda_0(T) + \Delta\lambda_r(\rho, T) + \Delta\lambda_C(\rho, T) \tag{15}$$

In Eq. (15), $\Delta\lambda_r$ (ρ, T) is the residual thermal conductivity, and $\Delta\lambda_C$(ρ, T) is the empirical critical enhancement.

The R134a is the reference fluid for the refrigerants [42], but for the hydrocarbons, it is better to consider propane or methane [45]. The viscosity and thermal conductivity of the other fluids are calculated from the properties of reference fluids. Critical properties of the fluid are required. Equation (16) presents the equation for the dynamic viscosity:

$$\eta(T) = \eta^{\circ}(T) + \Delta\eta^{R}\left(\frac{T}{f}, \rho h\right)F_{\eta} \tag{16}$$

In Eq. (16), $f = \frac{T_c}{T_c^R}$, $h = \frac{\rho_c^R}{\rho_c}$, and $F_{\eta} = f^{\frac{1}{2}}h^{-\frac{2}{3}}\left(\frac{M}{M^R}\right)^{\frac{1}{2}}$ reduction ratio. Equation (17) presents the equation for the thermal conductivity:

$$\lambda(T) = \lambda^{\circ}(T) + \Delta\lambda^{R}\left(\frac{T}{f}, \rho h\right) F_{\lambda} \tag{17}$$

In Eq. (17), $f = \frac{T_c}{T_c^R}$, $h = \frac{\rho_c^R}{\rho_c}$, and $F_\lambda = f^{\frac{1}{2}} h^{-\frac{2}{3}} \left(\frac{M^R}{M}\right)^{\frac{1}{2}}$ reduction ratio. For mixtures, mixing rules have to be considered [46].

6. Presentation of some results

In this section, we will present some results obtained for pure component (transport properties) and multicomponent systems (equilibrium properties) on working fluids already published.

6.1 Phase diagram

We will present the results obtained for three binary systems. The first one concerns a mixture of CO_2 and R1234ze(e) published by Wang et al. [12]). **Figure 14** presents the phase diagram. The system presents no azeotropic behavior. We can notice that with the experimental data, we can also predict a critical point using asymptotic laws of behavior [12]. **Figure 15** presents a comparison with the critical point measured by Juntaratchat et al. [50] using a critical point setup similar to the equipment already presented in Section 4.

The binary system R245fa + isopentane is presented on **Figure 16** at 392.87 K. Measurement was done using static-analytic method [51]. We have used REFPROP 10.0 to correlate the data (REFPROP 10.0 [52] uses Fundamental Helmholtz equation). We can observe a good agreement between REFPROP prediction and the experimental data (we have one comment concerning this point: the reference of the data used in the data treatment by REFPROP is not clearly mentioned).

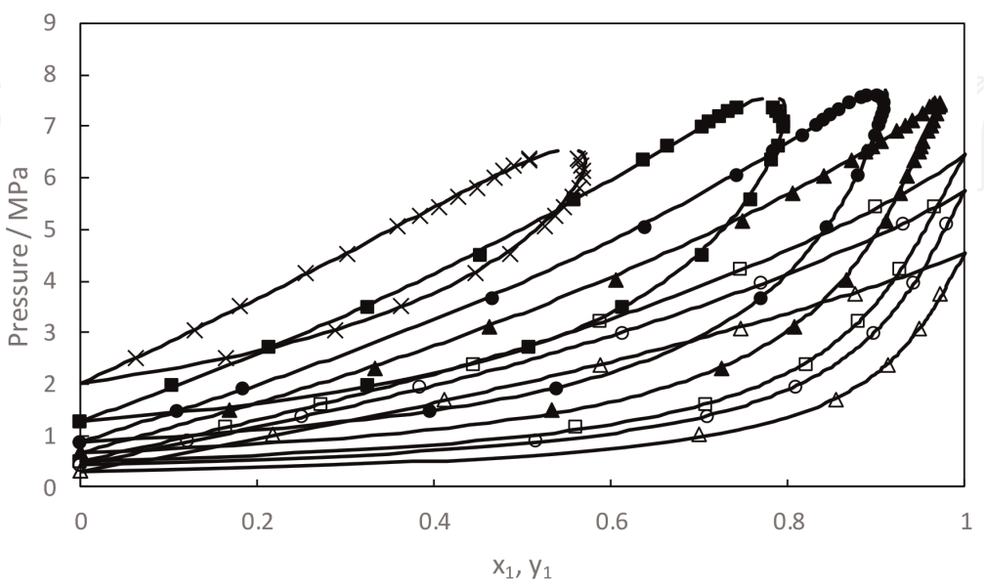

Figure 14.
Pressure as a function of CO_2 mole fraction in the CO_2. (1)—R-1234ze(E) and (2) mixture at different temperatures. Δ, 283.32 K; o, 293.15 K; □, 298.15 K; ▲, 308.13 K; ●, 318.11 K; ■, 333.01 K; ×, 353.02 K. Solid lines: calculated with Peng-Robinson EoS [47], Wong-Sandler mixing rules [48], and NRTL [49] activity coefficient model [12].

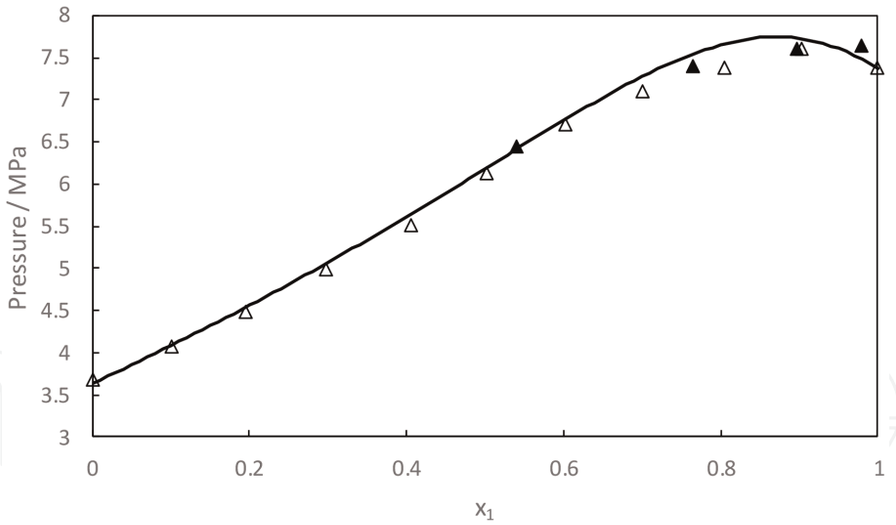

Figure 15.
Critical pressure of the binary system CO2 (1) +R-1234ze(E) (2) [12]. Solid line: calculated using PR EoS, Wong-Sandler mixing rules, and NRTL activity coefficient model. Δ, experimental data from Juntaratchat et al. [50]; ▲, predicted using power laws with asymptotic behavior at critical point.

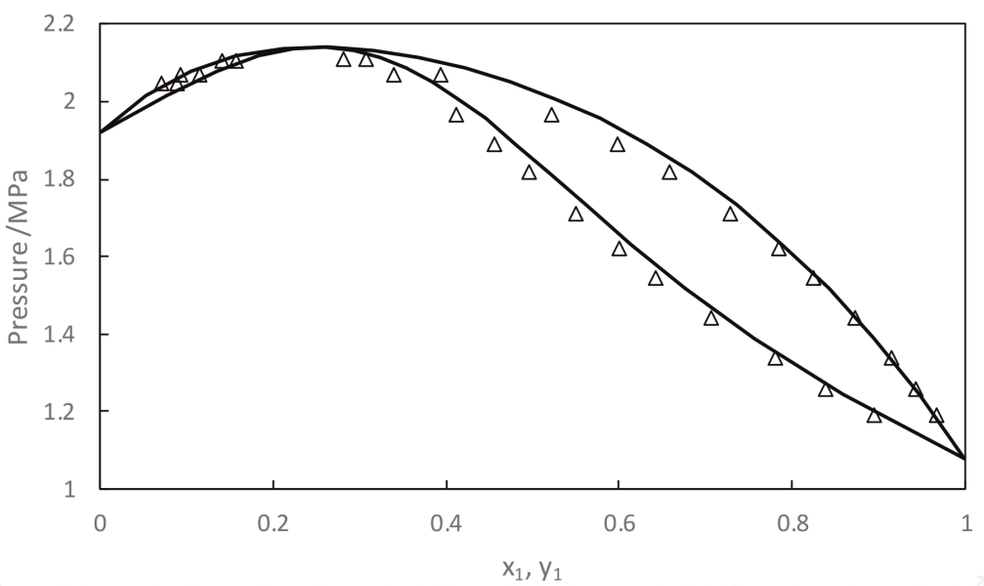

Figure 16.
Pressure as a function of CO2 mole fraction in the isopentane. (1) −R245fa and (2) mixture at 392.87 K. Comparison between experimental data [51] and modeling using REFPROP 10.0.

6.2 Bubble point

Variable volume cell was used to determine bubble pressure of the ternary system composed with R32 + R290 + R227ea [53]. **Figure 17** presents the results obtained. The data were correlated by a cubic equation of state (Redlich-Kwong-Soave EoS [54], MHV1 [55] mixing rules, and NRTL [49] activity coefficient model).

6.3 Densities

Vibrating tube densitometer technique was used to measure the densities of the R1216 [20]. The results are presented on **Figure 18**. The same technique is used to obtain density data of R1234yf (**Figure 19**) at saturation [56]. Density at the vicinity

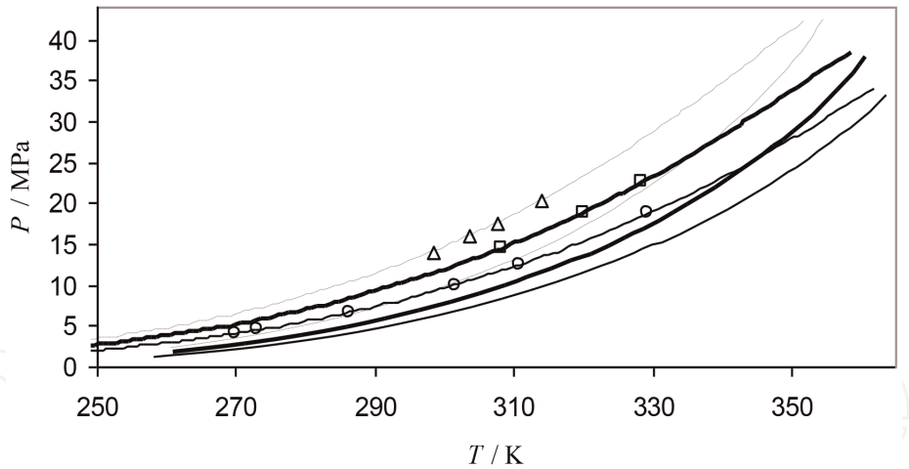

Figure 17.
The system R32 (1) +R290 (2) +R227ea (3) [53]. Pressure versus temperature diagram for each composition. Mixture 1: ×1 = 0.322, ×2 = 0.123, (□) experimental bubble points. Mixture 2: ×1 = 0.135, ×2 = 0.174, (○) experimental bubble points. Mixture 3: ×1 = 0.493, ×2 = 0.127, (Δ) experimental bubble points.

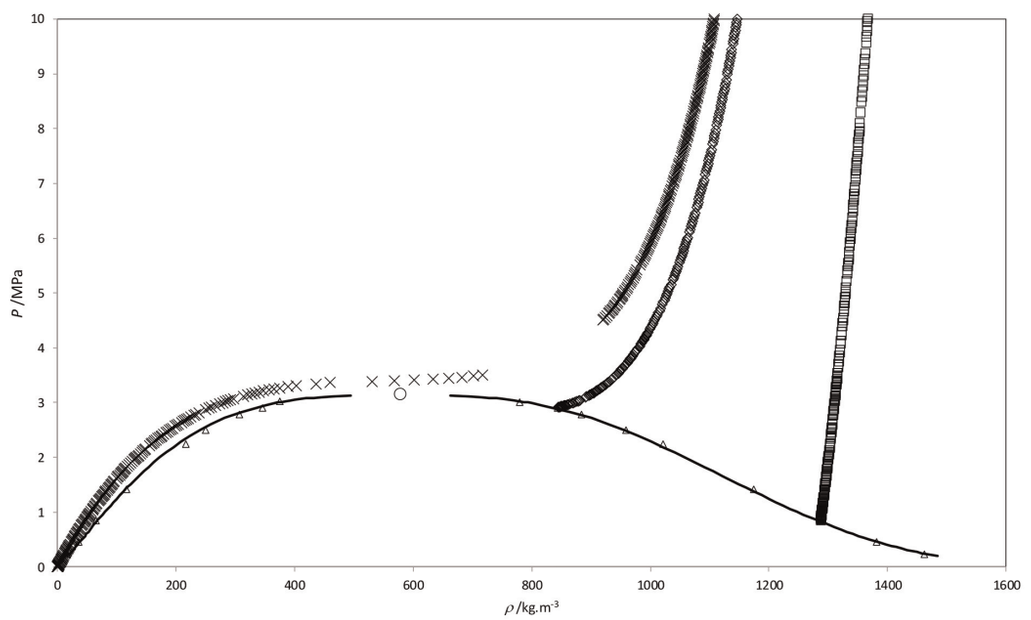

Figure 18.
Pressure density phase diagram of hexafluoropropene (R1216). (Δ), experimental densities at saturation; out of saturation; (×) 362.90 K; (◇) 355.18 K and (□) 303.28 K; O, critical point [20].

of the critical point was obtained by an isochoric method used by Tanaka and Higashi [21].

6.4 Dynamic viscosity

Capillary viscometer was used by Laesecke et al. [57] to determine the dynamic viscosity of liquid R245fa at saturation. **Figure 20** presents the results and comparison with prediction using REFPROP 10.0. A good agreement is observed.

6.5 Thermal conductivity

Marrucho et al. [58] have used the transient hot-wire technique to measure the thermal conductivity of R365mfc. **Figure 21** presents the results obtained at 336.85

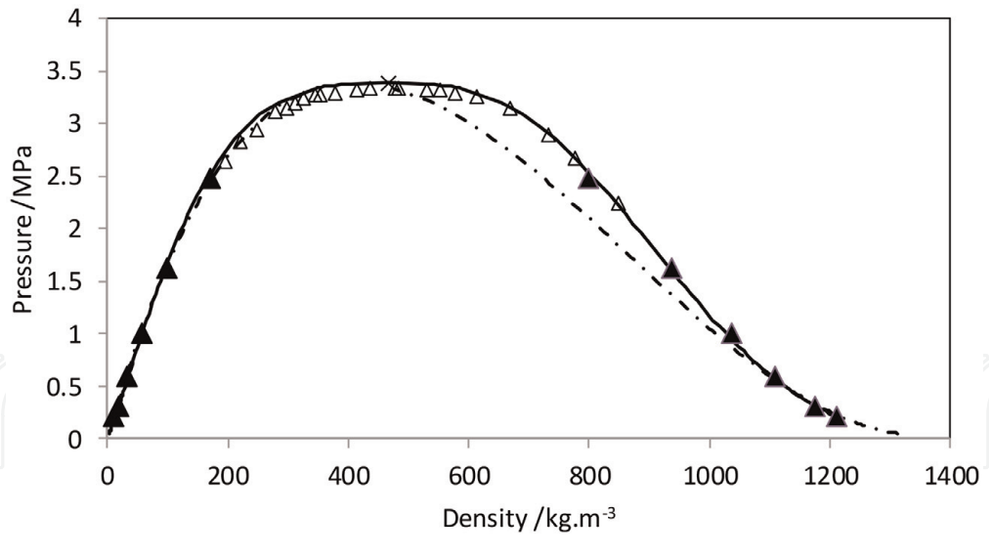

Figure 19.
Pressure density phase diagram of R1234yf at saturation. (Δ) data from Tanaka and Higashi [X], (▲) Coquelet et al. [56], (×) critical point from REFPROP. Solid line, correlation presented in Coquelet et al. [20]; (—·), Peng-Robinson EoS.

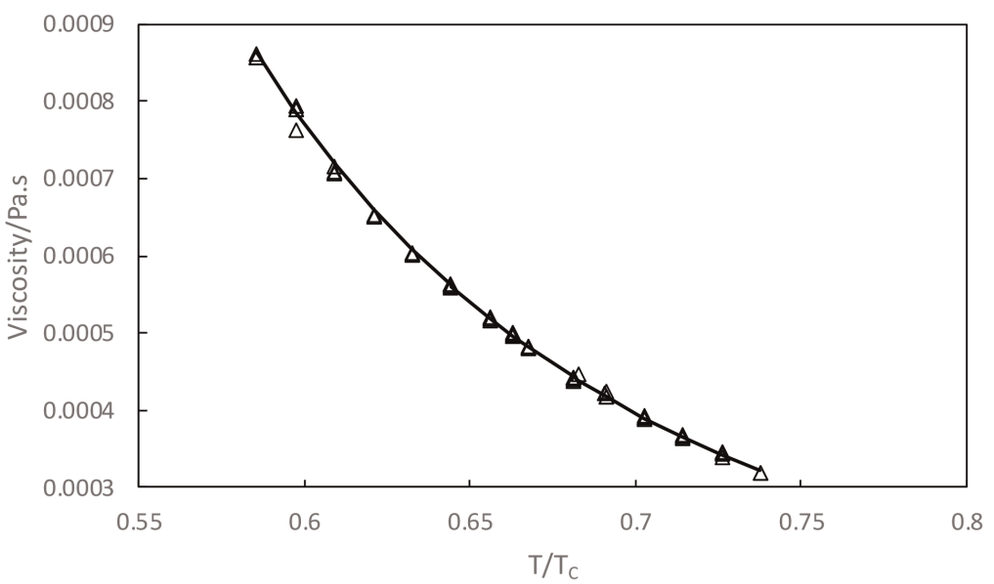

Figure 20.
Dynamic viscosity of R245fa at saturation. Symbol: experimental data from Laesecke et al. [57]. Solid line: prediction using REFPROP 10.0.

and 377.4 K for several pressures from 1 to 4.5 bar. Comparison was done with prediction from REFPROP 10.0. A good agreement is observed.

7. Conclusion

The optimization of ORC depends strongly on the capability of models to predict the thermophysical properties of working fluids for their selection and retrofit in existing ORC equipment. The main thermophysical properties include phase equilibria (and so critical point), densities, speed of sound, dynamic viscosity, and thermal conductivity. Through this book chapter, the reader can easily understand that several experimental techniques developed to measure the thermophysical properties exist. Some of them were presented and described. In general, these

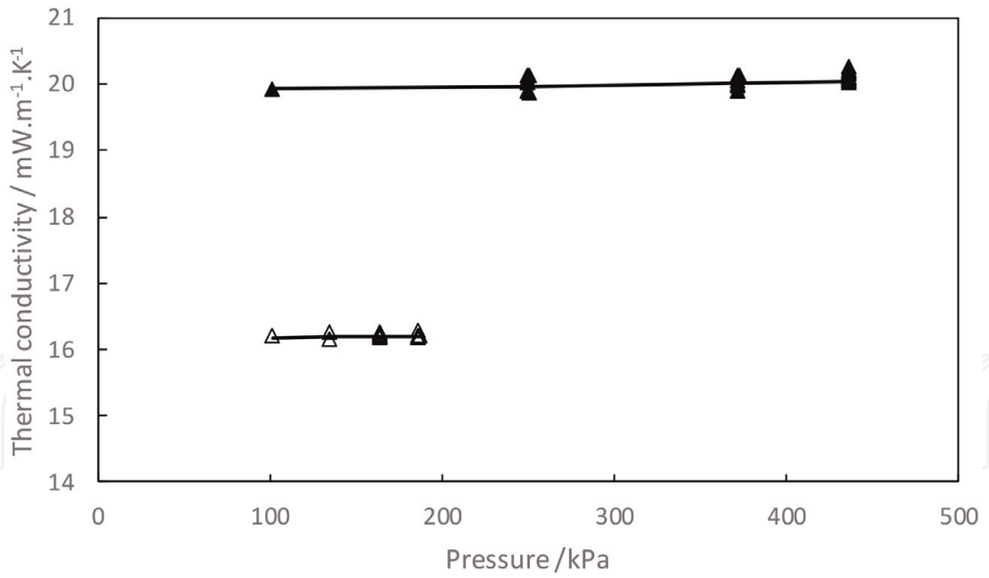

Figure 21.
Thermal conductivity of R365mfc as a function of pressure. Symbol: experimental data from Marrucho et al. [58] at (Δ) 336.85 K and (▲) 377.40 K. Solid line: prediction using REFPROP 10.0.

techniques are very accurate, and we recommend to use the experimental technique with which the operator/engineer is the most familiar with. It is obvious to see that we have the capability to determine all the thermophysical properties of interest for the design and optimization of ORC. In our opinion, there are two main challenges for the future. The first one concerns the development of equipment which permits the determination of several thermophysical properties together and particularly thermophysical properties at equilibrium. The second one concerns the development of equipment which require a small quantity of sample and so the utilization of in situ analysis techniques. In effect, it is difficult to have important quantity of new synthesis molecules (with high purity) to realize the measurement of accurate thermophysical properties of pure components and mixtures. The experimental data will be used to adjust parameters on models or correlations. Data acquisition is an essential step for a good working fluid design. In the literature an optimal selection (**Figure 22**) of working fluids as a function of the temperature of the heating medium exists [59]. This classification does not concern mixtures, and in the case of the utilization of mixtures, experimental characterization has to be done.

Temperature /K						
320	365	395	420	445	465	500
R134a	R22	R152a	R600a	R600		R123
R32	R290	R124	R142b	R254fa		R365mfc
	R134a	CF3I	R236a	Néopentene		R601a
		R236fa	Isobutene	R245ca		R601
			Butene			R141b

Figure 22.
Some working fluid for several level of temperature of heating medium [59].

Author details

Christophe Coquelet*, Alain Valtz and Pascal Théveneau
CTP-Centre of Thermodynamics of Processes, Mines ParisTech, PSL University, France

*Address all correspondence to: christophe.coquelet@mines-paristech.fr

IntechOpen

References

[1] Badr O, Probert SD, O'Callaghan PW. Selecting a working fluid for a Rankine cycle engine. Applied Energy. 1985;**21**:1-42. DOI: 10.1016/0306-2619(85)90072-8

[2] Saleh B, Kogalbauer G, Wendland M, Fischer J. Working fluids for low temperature organic Rankine cycles. Energy. 2007;**32**:1210-1221. DOI: 10.1016/j.energy.2006.07.001

[3] Maizza V, Maizza A. Unconventional working fluids in organic Rankine Cycles for waste energy recovery systems. Applied Thermal Engineering. 2001;**21**:381-390. DOI: 10.1016/S1359-4311(00)00044-2

[4] Liu B, Riviere P, Coquelet C, Gicquel R, David F. Investigation of a two stage Rankine cycle of electricity power plants. Applied Energy. 2012;**100**: 285-294. DOI: 10.1016/j.apenergy.2012.05.044

[5] Rahbar K, Mahmoud S, Al-Dadah RK, Moazami N, Mirhadizadeh SA. Review of organic Rankine cycle for small-scale applications. Energy Conversion and Management. 2017;**134**: 135-155. DOI: 10.1016/j.enconman.2016.12.023

[6] Liu B. Modélisation d'un cycle de production d'électricité bi-étagé à aeroréfrigérant sec [thesis]. MinesParisTech; 2014

[7] Bolaji BO. Experimental study of R152a and R32 to replace R134a in a domestic refrigerator. Energy. 2010; **35**(9):3793-3798. DOI: 10.1016/j.energy.2010.05.031

[8] Privat R, Jaubert JN. Classification of global fluid-phase equilibrium behaviors in binary systems. Chemical Engineering Research and Design. 2013; **91**:1807-1839. DOI: 10.1016/j.cherd.2013.06.026

[9] Scott RL, van Konynenburg PH. Critical lines and phase equilibria in binary van der Waals mixtures. Philosophical Transactions of the Royal Society. 1980;**298**:495-594. DOI: 10.1098/rsta.1980.0266

[10] Galicia-Luna LA, Richon D, Renon H. New loading technique for a vibrating tube densimeter and measurements of liquid densities up to 39.5 MPa for binary and ternary mixtures of the carbon dioxide-methanol-propane system. Journal of Chemical and Engineering Data. 1994; **39**(3):424-431. DOI: 10.1021:je00015a005

[11] Bouchot C, Richon D. Direct pressure−volume−temperature and vapor−liquid equilibrium measurements with a single equipment using a vibrating tube densimeter up to 393 K and 40 MPa: description of the original apparatus and new data. Industrial & Engineering Chemistry Research. 1998;**37**(8):3295-3304. DOI: 10.1021/ie970804w

[12] Wang S, Fauve R, Coquelet C, Valtz A, Houriez C, Artola PA, et al. Vapor–liquid equilibrium and molecular simulation data for carbon dioxide (CO_2) + trans-1, 3, 3, 3-tetrafluoroprop-1-ene (R-1234ze (E)) mixture at temperatures from 283.32 to 353.02 K and pressures up to 7.6 MPa. International Journal of Refrigeration. 2019;**98**:362-371. DOI: 10.1016/j.ijrefrig.2018.10.032

[13] Meskel-Lesavre M, Richon D, Renon H. A new variable volume cell for determining vapor-liquid equilibria and saturated liquid molar volume by the static method. Industrial and Engineering Chemistry Fundamentals. 1981;**20**: 284-289. DOI: 10.1021:i100003a017

[14] Fontalba F, Richon D, Renon H. Simultaneous determination of PVT and

VLE data of binary mixtures up to 45 MPa and 433 K: A new apparatus without phase sampling and analysis. The Review of Scientific Instruments. 1984;**55**:944-951. DOI: 10.1063/1.1137870

[15] Tzirakis F, Stringari P, Von Solms N, Coquelet C, Kontogeorgis G. Hydrate equilibrium data for the CO_2+ N_2 system with the use of tetra-n-butylammonium bromide (TBAB), cyclopentane (CP) and their mixture. Fluid Phase Equilibria. 2016;**2016, 408**:240-247. DOI: 10.1016/j.fluid.2015.09.021

[16] Wagner W, Brachthäuser K, Kleinrahm R, Lösch HW. A new, accurate single-sinker densitometer for temperatures from 233 to 523 K at pressures up to 30 MPa. International Journal of Thermophysics. 1995;**16**(2): 399-411. DOI: 10.1007/BF01441906

[17] Bridgman PW. The volume of eighteen liquids as a function of pressure and temperature. Proceedings of the American Academy of Arts and Sciences. 1931;**66**(5):185-233. DOI: 10.2307/20026332

[18] Straty GC, Palavra AMF. Automated high temperature PVT apparatus with data for propane. Journal of Research of the National Bureau of Standards. 1984; **89**(5):375-383

[19] Goodwin ARH, Marsh KN, Wakeham WA. Measurement of the Thermodynamic Properties of Single Phases, Experimental Thermodynamics Vol VI IUPAC. Amsterdam: Elsevier; 2003

[20] Coquelet C, Ramjugernath D, Madani H, Valtz A, Naidoo P, Meniai AH. Experimental measurement of vapor pressures and densities of pure hexafluoropropylene. Journal of Chemical & Engineering Data. 2010;**55**(6): 2093-2099. DOI: 10.1021/je900596d

[21] Tanaka K, Higashi Y. Thermodynamic properties of HFO-1234yf (2, 3, 3, 3-tetrafluoropropene). International Journal of Refrigeration. 2010;**33**(3):474-479. DOI: 10.1016/j.ijrefrig.2009.10.003

[22] Moldover MR, Mehl JB, Greenspan M. Gas-filled spherical resonators: Theory and experiment. The Journal of the Acoustical Society of America. 1986; **79**(2):253-272. DOI: 10.1121/1.393566

[23] Trusler JPM, Zarari M. The speed of sound and derived thermodynamic properties of methane at temperatures between 275 and 375 K and pressures up to 10 MPa. The Journal of Chemical Thermodynamics. 1992;**24**(9): 973-991. DOI: 10.1016/S0021-9614(05) 80008-4

[24] Benedetto G, Gavioso RM, Spagnolo R, Marcarino P, Merlone A. Acoustic measurements of the thermodynamic temperature between the triple point of mercury and 380 K. Metrologia. 2004; **41**(1):74-98

[25] Ahmadi P, Chapoy A, Tohidi B. Density, speed of sound and derived thermodynamic properties of a synthetic natural gas. Journal of Natural Gas Science and Engineering. 2017;**40**: 249-266. DOI: 10.1016/j.jngse.2017.02. 009Get

[26] Al Ghafri SZ, Rowland D, Akhfash M, Arami-Niya A, Khamphasith M, Xiao X, et al. Thermodynamic properties of hydrofluoroolefin (R1234yf and R1234ze (E)) refrigerant mixtures: Density, vapour-liquid equilibrium, and heat capacity data and modelling. International Journal of Refrigeration. 2019;**98**:249-260. DOI: 10.1016/j. ijrefrig.2018.10.027

[27] Calvignac B, Rodier E, Letourneau JJ, Vitoux P, Aymonier C, Fages J. Development of an improved falling ball viscometer for high-pressure measurements with supercritical CO_2. The Journal of Supercritical Fluids. 2010;**55**(1):96-106. DOI: 10.1016/j. supflu.2010.07.012

[28] Daridon JL, Cassiède M, Paillol JH, Pauly J. Viscosity measurements of liquids under pressure by using the quartz crystal resonators. Review of Scientific Instruments. 2011;**82**(9):095114. DOI: 10.1063/1.3638465

[29] Caudwell D, Goodwin AR, Trusler JM. A robust vibrating wire viscometer for reservoir fluids: results for toluene and n-decane. Journal of Petroleum Science and Engineering. 2004;**44**(3–4): 333-340. DOI: 10.1016/j.petrol.2004.02.019

[30] El Abbadi J. Thermodynamic properties of new refrigerants [thesis]. Mines ParisTech; 2016

[31] Le N, Viscosité B. Définitions et dispositifs de mesure. Techniques de l'ingénieur. Constantes physico-chimiques. 2004:3K478

[32] Kashefi K, Chapoy A, Bell K, Tohidi B. Viscosity of binary and multicomponent hydrocarbon fluids at high pressure and high temperature conditions: Measurements and predictions. Journal of Petroleum Science and Engineering. 2013;**112**: 153-160. DOI: 10.1016/j.petrol.2013.10.021

[33] Tait RWF, Hills BA. Methods for determining liquid thermal conductivities. Industrial and Engineering Chemistry. 1964; **56**(7):29-35. DOI: 10.1021:ie50655a005

[34] Healy JJ, De Groot JJ, Kestin J. The theory of the hot-wire method for measuring thermal conductivity. Physica C. 1976;**82**(2):392-408. DOI: 10.1016/0378-4363(76)90203-5

[35] Marsh KN, Perkins RA, Ramires MLV. Measurement and correlation from 86 to 600K at pressures to 70 MPa. Journal of Chemical & Engineering Data. 2002;**47**:932-940. DOI: 10.1021/je010001m

[36] Chapman WG, Gubbins KE, Jackson G, Radosz M. SAFT: Equation-of-state solution model for associating fluids. Fluid Phase Equilibria. 1989;**52**: 31-38. DOI: 10.1016/0378-3812(89)80308-5

[37] Gil-Villegas A, Galindo A, Whitehead PJ, Mills SJ, Jackson G, Burgess AN. Statistical associating fluid theory for chain molecules with attractive potentials of variable range. The Journal of Chemical Physics. 1997;**106**(10):4168-4186. DOI: 10.1063/1.473101

[38] Gross J, Sadowski G. Perturbed-chain SAFT: An equation of state based on a perturbation theory for chain molecules. Industrial & Engineering Chemistry Research. 2001;**40**(4): 1244-1260. DOI: 10.1021/ie0003887

[39] Lafitte T, Apostolakou A, Avendano C, Galindo A, Adjiman CS, Müller EA, et al. Accurate statistical associating fluid theory for chain molecules formed from Mie segments. The Journal of Chemical Physics. 2013;**139**(15):154504. DOI: 10.1063/1.4819786

[40] Tillner-Roth R. Die thermodynamischen Eigenschaften von R 152a, R 134a and ihren Gemischen-Messungen Und Fundamentalgleichungen PhD. Germany: University of Hannover; 1993

[41] Mac Linden MO, Klein SA. A next generation refrigerant properties database. In: International Refrigeration and Air Conditioning conference 1996: paper 357. pp. 409-414

[42] Huber ML, Laesecke A, Perkins RA. Model for the viscosity and thermal conductivity of refrigerants, including a new correlation for the viscosity of R134a. Industrial & Engineering Chemistry Research. 2003;**42**: 3163-3178. DOI: 10.1021/ie0300880

[43] Klein SA, McLinden MO, Laesecke A. An improved extended

corresponding states method for estimation of viscosity of pure refrigerants and mixtures. International Journal of Refrigeration. 1997;**20**(3): 208-217. DOI: 10.1016/S0140-7007(96) 00073-4

[44] Poling E, Prausnitz JM. The Properties of Gases and Liquids. McGraw-Hill Professional. New York: Mcgraw-Hill; 2000

[45] Huber ML, Hanley HJM. The Corresponding-States Principle: Dense Fluids. Transport Properties of Fluids. Cambridge University Press, IUPAC; 1996. pp. 283-296

[46] Ely JF, Huber ML. A predictive extended corresponding states model for pure and mixed refrigerants including a new equation of state for R134a. International Journal of Refrigeration. 1994;**17**:18-31. DOI: 10.1016/0140-7007(94)90083-3

[47] Peng DY, Robinson DB. A new two-constant equation of state. Industrial and Engineering Chemistry Fundamentals. 1976;**15**(1):59-64. DOI: 10.1021:i160057a011

[48] Wong DSH, Sandler SI. A theoretically correct mixing rule for cubic equations of state. AICHE Journal. 1992;**38**(5):671-680. DOI: 10.1002: aic.690380505

[49] Renon H, Prausnitz JM. Local compositions in thermodynamic excess functions for liquid mixtures. AICHE Journal. 1968, 1968;**14**(1):135-144. DOI: 10.1002/aic.690140124

[50] Juntarachat N, Valtz A, Coquelet C, Privat R, Jaubert JN. Experimental mea surements and correlation of vapor-liquid equilibrium and critical data for the CO_2 + R1234yf and CO_2 + R1234ze (E) binary mixtures. International Journal of Refrigeration. 2014;**47**: 141-152. DOI: 10.1016/j.ijrefrig.2014. 09.001

[51] El Ahmar E, Valtz A, Paricaud P, Coquelet C, Abbas L, Rached W. Vapour–liquid equilibrium of binary systems containing pentafluorochemicals from 363 to 413 K: Measurement and modelling with Peng–Robinson and three SAFT-like equations of states. International Journal of Refrigeration. 2012;**35**(8):2297-2310. DOI: 10.1016/j.ijrefrig.2012.05.016

[52] Lemmon EW, Bell IH, Huber ML, McLinden MO. NIST standard reference database 23: Reference fluid thermodynamic and transport properties-REFPROP (National Institute of Standards and Technology, Boulder, CO) 2018: Version 10.0

[53] Coquelet C, Chareton A, Richon D. Vapour–liquid equilibrium measurements and correlation of the difluoromethane (R32) + propane (R290) + 1, 1, 1, 2, 3, 3, 3-heptafluoropropane (R227ea) ternary mixture at temperatures from 269.85 to 328.35 K. Fluid Phase Equilibria. 2004; **218**(2):209-214. DOI: 10.1016/j. fluid.2003.12.009

[54] Soave G. Equilibrium constants from a modified Redlich-Kwong equation of state. Chemical Engineering Science. 1972;**27**(6):1197-1203. DOI: 10.1016/0009-2509(72)80096-4

[55] Michelsen ML. A modified Huron-Vidal mixing rule for cubic equations of state. Fluid Phase Equilibria. 1990;**60** (1–2):213-219. DOI: 10.1016/0378-3812 (90)85053-D

[56] Coquelet C, Valtz A, Théveneau P. Personal Communication and Confidential Data

[57] Laesecke A, Hafer RF. Viscosity of fluorinated propane isomers. 2. Measurements of three compounds and model comparisons. Journal of Chemical & Engineering Data. 1998;**43**(1):84-92. DOI: 10.1021/je970186q

[58] Marrucho IM, Oliveira NS, Dohrn R. Vapor-phase thermal conductivity, vapor pressure, and liquid density of R365mfc. Journal of Chemical & Engineering Data. 2002;**47**(3):554-558. DOI: 10.1021/je015534

[59] Wang D, Ling X, Peng H, Liu L, Tao L. Efficiency and optimal performance evaluation of organic Rankine cycle for low grade waste heat power generation. Energy. 2013;**50**:343-352. DOI: 10.1016/j.energy.2012.11.010